Thickness dependence of magnetic relaxation and E-J characteristics in superconducting (Gd-Y)-Ba-Cu-O films with strong vortex pinning

Ö. Polat,[1,2] J. W. Sinclair,[2] Y. L. Zuev,[2] J. R. Thompson,[1,2,*] D. K. Christen,[1] S. W. Cook,[1] D. Kumar,[3] Yimin Chen,[4] and V. Selvamanickam[4]

[1]*Materials Science and Technology Division, Oak Ridge National Laboratory, Oak Ridge, Tennessee 37831-6092, USA*
[2]*Department of Physics, The University of Tennessee, Knoxville, Tennessee 37996-1200, USA*
[3]*Department of Mechanical Engineering, NC A&T University, Greensboro, North Carolina, USA*
[4]*SuperPower, Inc., 450 Duane Ave., Schenectady, New York 12304, USA*

The dependence of the critical current density J_c on temperature, magnetic field, and film thickness has been investigated in (Gd-Y)-Ba-Cu-O materials of 0.7, 1.4, and 2.8 μm thickness. Generally the J_c decreases with film thickness at investigated temperatures and magnetic fields. The nature and strength of the pinning centers for vortices have been identified through angular and temperature measurements, respectively. These films do not exhibit c-axis correlated vortex pinning, but do have correlated defects oriented near the ab planes. For all film thicknesses studied, strong pinning dominates at most temperatures. The vortex dynamics were investigated through magnetic relaxation studies in the temperature range of 5–77 K in 1 and 3 T applied magnetic fields, $H \parallel$ surface normal. The creep rate S is thickness dependent at high temperatures, implying that the pinning energy is also thickness dependent. Maley analyses of the relaxation data show an inverse power law variation for the effective pinning energy $U_{\text{eff}} \sim (J_0/J)^{\mu}$. Finally, the electric field-current density (E-J) characteristics were determined over a wide range of dissipation by combining experimental results from transport, swept field magnetometry (VSM), and superconducting quantum interference device (SQUID) magnetometry. We develop a self-consistent model of the combined experimental results, leading to an estimation of the critical current density $J_{c0}(T)$ in the absence of flux creep.

PACS number(s): 74.25.Sv, 74.25.Wx, 74.78.−w

I. INTRODUCTION

Second generation (2G) coated conductors, based on the high-temperature superconductors (Y-RE)Ba$_2$Cu$_3$O$_7$, are beginning to meet industrial demands for high critical currents I_c for applications such as motors, transformers, and generators. As such, they are expected to have a major impact internationally on the supply and utilization of electrical energy. In a superconducting tape, an obvious and seemingly straightforward method to increase the I_c is to increase the thickness of the high-T_c superconductor (HTS) layer. However, it has been found that the *density* of critical currents J_c often decreases significantly as the film thickness d is increased.[1–10] On the other hand, such a falloff is hardly universal and materials with thickness-insensitive or thickness-independent J_c have been synthesized using several synthesis approaches, including Ba-F based methods,[11,12] hybrid liquid phase epitaxy,[13] and pulsed laser deposition for interface control as well as HTS deposition.[14] While the technical progress in developing these "coated conductors" has been impressive, there remain many fundamental questions in the basic physical understanding of the underlying processes that govern the flow of critical currents in these scientifically interesting materials. The overall objective of this work is to make a multifaceted, reasonably self-consistent investigation of HTS materials containing precipitates that provide strong vortex pinning.

A falloff in J_c with increasing layer thickness is widely observed, although not ubiquitous. Such a decrease can arise from defective materials, changes in the physical processes governing current transport, or some combination of these.

Possible material issues contributing to a degradation in J_c may include changes in the microstructure as the HTS becomes thicker; these include a-axis growth and the formation of secondary phases, voids, etc. Increasing porosity and lack of flux pinning centers also can be important factors in the decrease of J_c with thickness. However, even though Foltyn *et al*.[15] successfully eliminated porosity problems by using smoother metal substrates, a decrease with thickness was nonetheless still observed. One well-documented mechanism leading to a falloff with thickness is the presence of additional pinning near the interface between the substrate and the superconductor, arising from a proliferation of misfit dislocations.[16] The effect of this "excess pinning" is most pronounced and visible, however, for HTS thicknesses below ∼0.7 μm, which is the minimum thickness used in most technological applications and is the thinnest material investigated in the present study. Overall, there is a prevalent viewpoint that J_c frequently decreases with thickness regardless of deposition method and substrate, even though problems with microstructure are improved or eliminated.

To understand the physical basis for a thickness dependent J_c, Gurevich[17] proposed a theoretical picture with vortex pinning by finite sized defects that can have some level of spatial correlation. According to this approach, the pinning of vortices perpendicular to the film surface depends on the vortex length d in comparison with the bulk pinning correlation length along the field direction. Hence there can be a 2D-3D crossover in vortex pinning, which yields a monotonic decrease of J_c with film thickness. An alternative explanation of the thickness dependence has been given by Sanchez *et al*., where the observed low-field J_c is suppressed by the effects of

the current-induced self-field.[18] According to those findings, for given pinning the high-field J_c would be unaffected by film thickness. Hence, it is of interest to further explore and clarify the possible mechanism(s) responsible for the observed thickness dependence of the strong-pinning systems that are exemplified by the 2G coated conductors investigated here.

In general, a better understanding of vortex-vortex and vortex-defect interactions provides a pathway for improving the performance of well textured HTS materials. The study of vortex physics is interesting, because the behavior of vortices governs the physical properties of superconductors, including the maximum electric current that can be supported. A key question for investigation is how the superconducting mixed state is changed when a transport current is applied. If vortices are forced to move, the motion leads to energy dissipation; thus heating is inevitable, unless the vortices are immobilized ("pinned") by inhomogeneities in the material that occur naturally or by artificial engineering. In fact, vortex motion (accompanied by power dissipation) often occurs easily in HTS materials due to a combination of high anisotropy and a short coherence length that enhances the effect of thermal fluctuations of the vortices. This thermal activation leads to strong magnetic relaxation (decay of persistent supercurrents with time) and it limits the current-carrying capacity of these materials. The mobile vortices in the media create an electric field E parallel to the current density J, which causes power dissipation in the material. Indeed, the associated E-J characteristics encapsulate many electrodynamical properties of a HTS material. Often the $E(J)$ characteristics can be approximated by a power-law relation, $E \sim J^n$, as observed in magnetic and transport measurements.[19–25]

In this study we have investigated the dependence of the critical current density of (Gd-Y)-Ba-Cu-O thin films as a function of film thickness, applied magnetic field, and temperature. Our results showed that the J_c decreases with film thickness. Measurements of the field dependence of J_c revealed a power-law variation at intermediate fields with $J_c \propto H^{-\alpha}$, where the values for the exponent α at high temperatures vary with thickness. Analysis of the temperature dependence of J_c indicates that for all materials studied, strong pinning effects dominate at nearly all temperatures.

These studies combine three different measurement techniques: conventional electrical transport, vibrating sample magnetometry (VSM), and SQUID magnetometer. Each of these operates in a different window of electric field E, and their combination was used to investigate the thickness dependence of the current-carrying properties of the (Gd-Y)-B-C-O thin films, including J_c, $E(J)$ characteristics, and creep behavior. Increasing the HTS thickness may affect these properties through changes in pinning dynamics or alterations in the vortex pinning landscape, or combinations of these. In the present work, sequentially deposited materials with HTS thicknesses in the technologically important range from 0.7 to 2.8 μm were studied. As noted, the E-J characteristics provide a model-free summary of electromagnetic properties, so we performed such investigations over a wide temperature range, 5–77 K, in applied magnetic fields up to 3 T. The combination of experimental methods generated electric fields in the region from 10^{-5} to 10^{-13} V/cm and revealed *approximate* power-law behavior, but with substantial departures from a

pure dependence $E \sim J^n$. The experimental data are compared with models from collective-creep theory[26] and vortex-glass theory.[27–30] We also find that the power index n, a parameter describing the steepness of an E-J curve, changes with layer thickness; for a given field temperature, the thickest film has the highest n value and that value decreases with increasing temperature and magnetic field. Finally, we successfully model the E-J curves using collective creep formalism with values for the glassy parameter μ obtained from a "Maley analysis" of creep data.

We have also analyzed the magnetic relaxation rates in (Gd-Y)-Ba-Cu-O films of different thicknesses. Results show that the relaxation rate S at elevated temperatures is largest for the thinnest sample, implying that the pinning energy depends on the sample thickness. Moreover, we use the Maley analysis to determine the pinning energies of the specimens experimentally. Results demonstrated that U_{eff} increases with decreasing current density, which is a consequence of the glassiness of the HTS materials.

II. EXPERIMENTAL ASPECTS

The materials investigated were precommercial c-axis textured thin films of (Gd-Y)-Ba-Cu-O superconductor with thicknesses of 0.7, 1.4, and 2.8 μm. They were deposited on a Hastelloy substrate, which was coated with ion beam assisted deposition (IBAD) buffer layers. The HTS material was deposited sequentially using 1, 2, or 4 passes of one original buffered tape, where a portion of the tape was removed for study after each pass. The HTS material, prepared by SuperPower, Inc., contained an excess of Gd-Y. This produced $(Y\text{-}Gd)_2O_3$ precipitates, which were observed in transmission electron microscopy (TEM) as roughly equiaxed particles of ~ 8 nm diameter that tend to layer near the ab plane. These precipitates, along with some antiphase boundaries oriented near the c axis and point-like disorder, serve as flux pinning centers. No Zr doping was used, meaning that these materials do not contain strongly pinning, self-assembled $BaZrO_3$-based "columnar" defects oriented near the c axis. However, similarly synthesized materials may exhibit some angularly selective pinning near the c axis (due to other forms of correlate disorder), as is weakly evident in the results for J_c versus field orientation shown later. For magnetization studies, samples of 2×2 mm^2 were cut from the tape. Laser scribing was used to remove the material near the edges to eliminate any cracks or damage due to cutting. The transition temperature $T_c \cong$ 92 K for all investigated samples was determined from the disappearance of the Meissner state signal.

Contact-free magnetic investigations were conducted in two instruments: a SQUID based magnetometer, Quantum Design model MPMS-7 with a maximum field of 7 T and a vibrating sample magnetometer (VSM), Quantum Design PPMS with an 8 T maximum field. The current density was obtained from measurements of hysteretic magnetization loops $M(H)$. These data were analyzed using the "sandpile" critical state model;[31,32] for a rectangular sample with sides $b > a$, the current density (in cgs units) is given by

$$J_c = \frac{20\Delta M}{a(1 - a/3b)}. \tag{1}$$

Here ΔM is the hysteresis in the magnetization curve $M(H)$ as given by $\Delta M = (M^- - M^+)$ where M^- (M^+) is measured in decreasing (increasing) magnetic field history, respectively.

For magnetic relaxation measurements, a sample was first zero field cooled to a desired temperature. Before starting creep measurements, we insured that the samples were in the critical state by changing the magnetic field sufficiently to force flux penetration to the center of the sample. In the creep studies the applied magnetic field parallel to the c axis was increased from -1 up to $+1$ T and fixed there; and then the decay of magnetization $M(t)$ was measured for 1 h. Measurements for $M(t)$ were conducted for both increasing and decreasing field histories in the temperature range 5–77 K. A scan length of 3 cm was used to maintain the film in a highly homogeneous region of magnetic field.

As noted, the E-J characteristics were obtained over a quite wide range of dissipation levels by combining results from dc electrical transport, vibrating sample magnetometry in a swept magnetic field, and flux creep (current decay) measured in a fixed magnetic field.

Conventional transport measurements were carried out at 65 and 77 K in magnetic fields up to 1.5 T. The width of the sample was 4 mm and the distance between voltage contacts was 4 mm. Typical E-field levels are 1 μV/cm, which is the usual criterion for the critical current density. Transport measurements are most facile at high temperatures or large magnetic fields, where E can be measurably large without creating excessive dissipation. In transport studies the E field is typically higher than that obtained by magnetic measurements. Of course higher E fields cause more energy dissipation. Transport measurements have several advantages, including conceptual simplicity, clarity of end-to-end current path, and a well-defined orientation relative to a tilted magnetic field in angular studies.

On the other hand, magnetic measurements have certain advantages over transport measurements. The dissipation level tends to be self-limiting, thereby precluding the hazard of "burning out" or destroying a valuable sample. Also, transport measurements are often restricted to higher temperatures and lower currents, due to heating of the contacts. In contrast, magnetic measurements are readily extended to lower temperatures. In this study, a VSM was employed to measure the magnetic moment of a square sample, 2×2 mm^2, at a wide range of temperatures and magnetic fields. The applied magnetic field in the VSM was swept at a fixed, controlled rate in the range (200–10) Oe/s = (20–1) mT/s. This induced an electric field E around the perimeter of the sample whose average values is given by the SI expression

$$E = \frac{d\varphi/dt}{\text{perimeter}} = \frac{1}{\text{perimeter}} \frac{d}{dt}(\text{Area} \times \text{Magnetic field})$$
$$= \frac{a}{4}\left(\frac{dB}{dt}\right). \tag{2}$$

Typical electric fields were $E \sim 10^{-7}$–10^{-9} V/cm.

At still lower electric fields, the E-J characteristics of a regularly shaped sample can be obtained from creep measurements. Conceptually the current decay rate dJ/dt [where J is related to the magnetization via Eq. (1)] is proportional to the electric field in the sample. Hence, the induced electric field
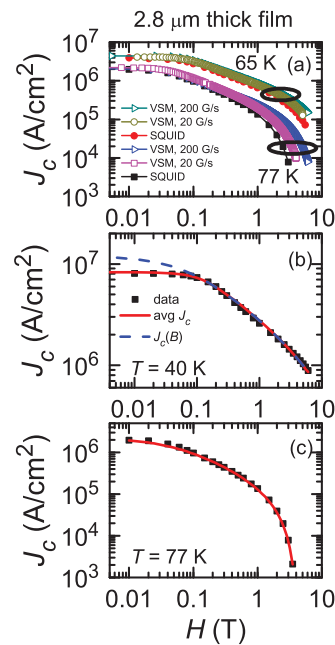

FIG. 1. (Color online) (a) The critical current density as a function of magnetic field, $H \parallel$ surface-normal, for a 2.8 μm thick (Gd-Y)-Ba-Cu-O film at 65 and 77 K. Values were determined at differing criteria for the effective electric field, using swept field VSM (200 and 20 Oe/s swept field rate), and SQUID-based magnetometry. (b) and (c) Results of fitting the phenomenological model [Eq. (4)] to SQUID magnetometry data at 40 and 77 K. The model describes the data particularly well at high temperatures, while low-temperature data require correction for self-field effects.

E averaged over the perimeter of the sample is given by (SI units)

$$E(J) = \frac{\pi a d}{12}\left(\frac{dJ}{dt}\right). \tag{3}$$

Here d is the HTS thickness and the width $a = 2$ mm. In creep measurements the electric fields typically lie in the range of 10^{-10}–10^{-13} V/cm.

III. RESULTS AND DISCUSSIONS

A. Field dependence of J_c

The field dependence of J_c at various temperatures (5–77 K) was obtained using transport, SQUID, and VSM methods. Figure 1(a) shows in log-log scales some representative results for J_c versus magnetic field obtained by VSM (for 200 and 20 Oe/s swept field rates) and SQUID magnetometer, for 2.8 μm thick films at 77 and 65 K. Qualitatively, the observed level of current density depends on the measurement method, which generates differing levels of electric field as described above; a quantitative analysis of their relationship will be presented later. In regard to the dependence on magnetic field, the first observation is that, in the low magnetic fields where each vortex can be individually pinned, J_c is independent of the applied magnetic field. This level region ends at a so-called characteristic or accommodation field H^*. At higher intermediate fields where $H_{\text{app}} > H^*$, interactions among the vortices are important and the density of vortices
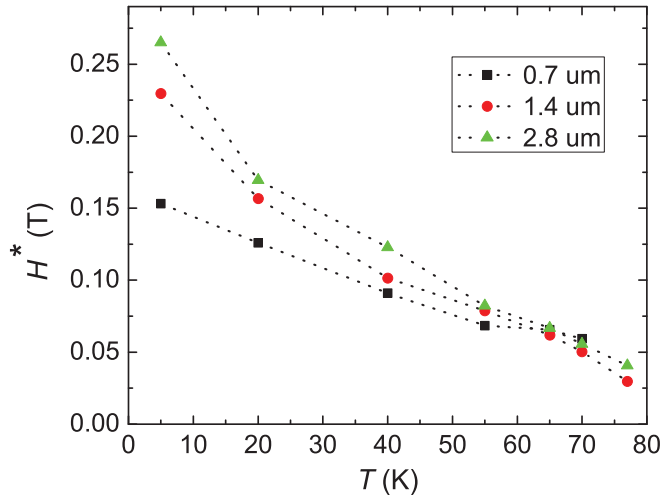
FIG. 2. (Color online) The thickness and temperature dependence of accommodation field H^* that marks the end of the low field region where J_c is insensitive to H_{app}. There is some dependence on thickness, which can be attributed in part to self-field effects.

FIG. 3. (Color online) Temperature dependence of the power-law exponent α that describes the falloff of J_c with magnetic field at intermediate field levels. Values shown were obtained (a) directly from log-log plots of the experimental data and (b) from fitting the model relation Eq. (4), respectively. The two sets of values for α differ somewhat, particularly at higher temperatures where effects of rapid creep and proximity to the irreversibility line become prominent. This leads to the temperature and thickness dependence observed in (a).

may become greater than that for the pinning centers. In this collective pinning regime, J_c falls off with field, often with an approximate power-law dependence $J_c \propto H^{-\alpha}$, where the exponent α depends on the pinning mechanism. Finally, when the applied field approaches the irreversibility field B_{irr}, the current density drops sharply due to a change in the pinning mechanism and/or accelerating flux creep.

The accommodation field H^* was determined by the intersection of the low-field level region and a power-law fit to the intermediate field regime.[33] The temperature dependence of H^* is shown in Fig. 2 for materials with three different thicknesses. Generally H^* decreases with increasing temperature. Some dependence on thickness is apparent, particularly at lower temperatures $T < \sim 40$ K. This may arise in part from effects of self-field, whose magnitude can be estimated as $B_{self} \approx \mu_o J_c d / 2$, where d is the thickness of the HTS film.[34] Thus thicker films and lower temperatures tend to produce higher B_{self} values. Consequently, self-field effects could mask the "intrinsic" accommodation field (i.e., that due only to the underlying pinning), when J_c is sufficiently large; more specifically, they can influence the overall field dependence of the macroscopic J_c averaged over the volume of the sample, where the critical current distribution within the material is affected in a self-consistent way by the local self-plus-applied field; this phenomenon is discussed further in the following paragraphs. At higher, intermediate fields where $H_{app} > H^*$, the J_c decays with a power-law field dependence as $J_c \propto H^{-\alpha}$. One can obtain values for the exponent α from the slopes in log-log plots like those in Fig. 1. The resulting experimental values for α lie in the range (0.48–0.94); Fig. 3(a) shows how the exponent α evolves with temperature for the three thicknesses. At low temperatures the values for α lie near $\frac{1}{2}$ and are very similar for the three specimens; in contrast, α becomes thickness sensitive at high temperatures. The thinnest film has highest α value (~ 0.94) at 77 K. Previously, it was shown that α increases as the electric field in the measurement decreases, with a logarithmic variation $\alpha \propto -\ln(E)$.[19] This effect may contribute to the observed dispersion at higher
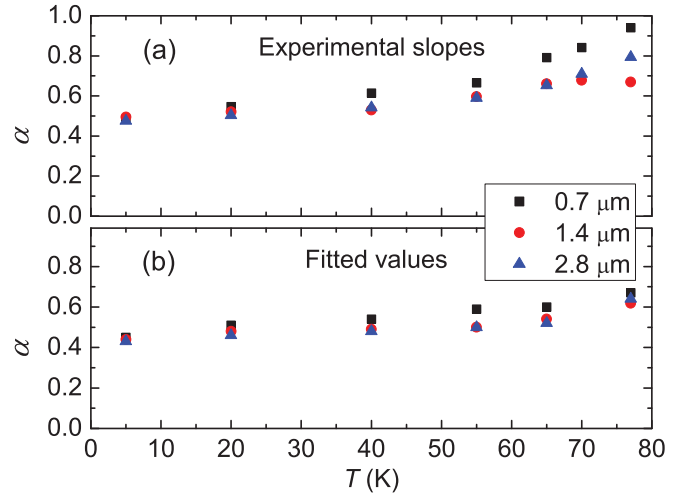
temperatures. However, flux creep typically accelerates with increasing field, particularly at higher temperatures, and this steepens the falloff of current density with field. As discussed later, creep at high temperatures is most pronounced in the thinnest film, which likely elevates the α slopes observed for it. At lower temperatures α becomes nearly independent of E.[19]

For the overall magnetic field dependence of J_c, Aytug *et al.* have described a useful phenomenological model with physically meaningful parameters.[35,36] In the following relationship (4), the first Kim-like factor provides a field-independent behavior in low fields and a crossover to a power law falloff at intermediate fields. The second factor incorporates the collapse of J_c when approaching the irreversibility field. The model expression provides

$$\frac{J_c(B)}{J_c(0)} = \left[1 + \frac{B}{B_0}\right]^{-\alpha} \left[1 - \frac{B}{B_{irr}}\right]^2. \quad (4)$$

Equation (4) adequately described the data of Refs. 35 and 36, where the film thickness of $\leqslant 0.3\ \mu$m limited the overall current levels. Here the experimental results for these thicker films are described reasonably well at high temperature. This is illustrated by the solid line in Fig. 1(c) showing a fit to the data at 77 K of the 2.8 μm thick sample. On the other hand, Eq. (4) describes the data at lower temperature only when the magnetic field is high [see Fig. 1(b)]. As the applied magnetic field decreases, the J_c data flatten quite abruptly compared with the more gradual curvature in Eq. (4) shown as a dashed line in Fig. 1(b). To understand the origin of this abrupt flattening, we have considered the nontrivial influence of the self-field. The solid curve in Fig. 1(b) results from a simple numerical, self-consistent treatment incorporating self-field effects that produce corrections to the bare model dependence described by Eq. (4), where the latter is shown as the dashed

curve. In previous work by others, the effects of self-field on the field dependence of J_c have been considered,[34,38] but were not applied for general values of α. Here we treat such effects in combination with the more generalized model, using a finite element approach for a long thin strip of superconductor. Overall, these self-organized effects tend to suppress and broaden the low-field J_c plateau without affecting the intermediate-to-high field dependence, as was found previously.[34,37–39] By allowing for self-field effects, the data of Fig. 1(b) can be reasonably well described by Eq. (4) over the entire field range.

In Eq. (4) the field B_0 sets the scale for the crossover from the field independent J_c (plateau region) to the power-law regime, presumably determined at the local level by the combined vortex-vortex and vortex-pinning interactions. While the fundamental significance of B_0 has been discussed from different viewpoints,[35,40] its relationship to the experimentally observed crossover field H^* will depend on additional mechanistic details. As might be expected, however, the fitted values for B_0 are comparable to but somewhat smaller than the experimentally observed H^*, as was also found previously.[36] The systematic effects of self-field corrections on this coupling between B_0 and H^* will not be pursued here, in part because of procedural problems in finding unique global fitting solutions using the present numerical techniques. The fitting procedure does, however, yield values for the exponent α, and these results are shown in Fig. 3(b) as a function of temperature. At low temperatures, the observed slopes α in Fig. 3(a) are very comparable with the fitted values in Fig. 3(b). Also, the fitted α values exhibit more limited thickness dependence at high temperatures, since the second factor in Eq. (4) accounts for most effects of fast creep near the irreversibility line. Indeed, we find that the α values so obtained span the range 1/2–5/8 as predicted theoretically for pinning by large sparse defects[41,42] such as the RE-oxide precipitates in these materials.

Now, let us discuss the irreversibility field B_{irr} that appears in the phenomenological expression Eq. (4). For most temperatures, this quantity is not directly measurable experimentally because B_{irr} is so large. Figure 4 exhibits the values deduced from fitting the data to the model relation Eq. (4). The inset shows that for a quite wide temperature range, $B_{\text{irr}}(T)$ varies smoothly with a dependence $\sim (1 - T/T_c)^2$ since the fitted straight line has a slope (1.95 ± 0.08) very near 2. Overall, with correction Eq. (4) provides a good description of the data at various temperatures. Since $J_c(0)$ can be measured either directly (in the absence of strong self-field effects) or obtained self-consistently (by including self-field corrections), the fits to Eq. (4) yield the three parameters B_0, α, and B_{irr} at each temperature and thickness. In terms of application of HTS coated conductors, such scaling gives a useful parametrization of the properties of those wires.

B. Field orientation and temperature dependence of J_c

For insight into the pinning of vortices in these (Gd-Y)-Ba-Cu-O samples, we studied the dependence of J_c on magnetic field orientation at 77 K in a 1 T applied field using traditional transport methods. Complementing this, we investigated the temperature dependence of J_c in a 1 T field parallel to c axis, using VSM methods.
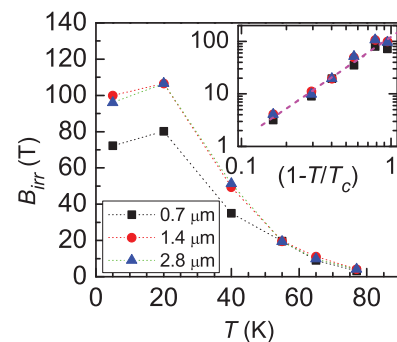

FIG. 4. (Color online) The irreversibility field B_{irr} vs T as obtained from fitting the model relation Eq. (4) to data like those in Figs. 1(b) and 1(c). At low temperatures B_{irr} increases significantly above usual measurement capabilities. Inset: a log-log presentation, where the fitted line shows B_{irr} varying as $(1 - T/T_c)^2$.

First, consider the dependence of J_c on orientation of the magnetic field, which helps to determine the nature of the defects present. Figure 5 shows the critical current density at 77 K and 1 T plotted versus field orientation angle θ. Angle θ is defined as the angle between the applied field and a line perpendicular to the plane of the superconductor. There is a sharp peak when the field is applied near the plane of the film. The offset of the peak from $\theta = 90°$ can be attributed to the fact that these materials commonly exhibit some tilting of the lattice planes and defect structures relative to the substrate;[43] hence the pronounced peaks at $\theta = 82$–85° arise from correlated disorder near the *ab* planes due to layering of the RE-oxide precipitates, stacking faults, or intergrowths,[44–46] perhaps with some contribution from intrinsic pinning. On the other hand, there is little to no structure in Fig. 5 when the field is applied near the c axis. Hence it can be said that none of the investigated samples has significant amounts of correlated disorder near the c axis. These results also imply that the nature of the defects does not change with thickness in the range investigated.
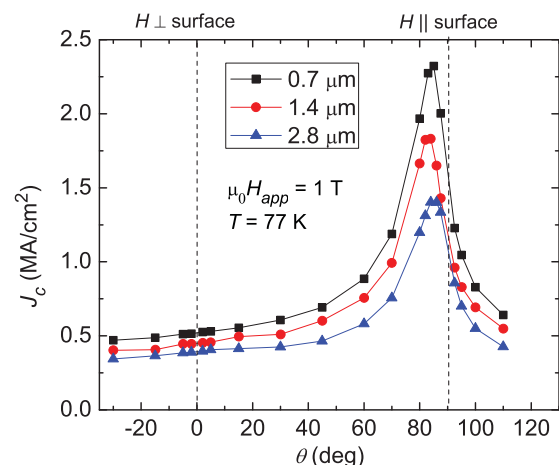

FIG. 5. (Color online) Dependence of the in-plane critical current density on orientation of the magnetic field for 0.7, 1.4, and 2.8 μm thick (Gd-Y)-Ba-Cu-O films at 77 K in 1 T applied magnetic field. Orientation of the field is measured from a line perpendicular to the surface. Units of J are MA/cm^2 = 10^6 A/cm^2.

Further information on the vortex pinning in the films was obtained from the temperature dependence of $J_c(T)$, measured by VSM in a 1 T field applied parallel to the c axis. It has been shown experimentally[47,48] and theoretically[49] that with weak pinning centers the J_c decays exponentially with temperature in HTS. This decay can be described by the following expression:

$$J_c^{\text{wk}}(T) = J_c^{\text{wk}}(0)\, e^{-(T/T_o)}.$$ (5)

Here $J_c^{\text{wk}}(0)$ is the contribution to J_c at 0 K by weak pinning defects (typically point-like disorder) and T_o relates their characteristic pinning energy. In HTS materials with strong pinning centers such as correlated defects, Nelson and Vinokur[50] and Hwa *et al.*[51] have predicted that J_c decays more slowly with a smoother temperature dependence, described by

$$J_c^{\text{str}}(T) = J_c^{\text{str}}(0)\, e^{-3(T/T^*)^2}.$$ (6)

Here $J_c^{\text{str}}(0)$ is the contribution of strong pinning centers to the J_c at 0 K and T^* characterizes the vortex pinning by strong defect centers. Experimental results have demonstrated that this model can be applied to HTS materials having strong pinning centers.[33,52–54]

Later, Plain *et al.* have shown a coexistence of both weak and strong pinning effects in melt-textured YBCO materials.[55] In order to describe their experimental data in the presence of such a complex pinning landscape, they assumed that the current densities in Eqs. (5) and (6) could be summed. (More properly, one should sum the pinning forces acting on the interacting array of vortices, but this is an extremely complex problem and theoretically intractable at present. Hence we use the simplified approximation of Plain *et al.* to gain some broad scale characterization of the pinning.) Thus one has

$$J_c(T) = J_c^{\text{wk}}(0)\, e^{-(T/T_o)} + J_c^{\text{str}}(0)\, e^{-3(T/T^*)^2}.$$ (7)

By fitting this expression to temperature dependent data for J_c at 1 T with $H \perp$ tape, we obtain the results shown in Figs. 6(a)–6(c) for the materials of differing thicknesses. Solid lines show the overall fitted curve, and the broken lines show the individual contributions from the first and second terms in Eq. (7). Note that at low temperatures, weak pinning from point-like disorder often contributes significantly to the J_c; for the present materials, however, the strong pinning component dominates for $T > \sim 20$ K. This strong pinning can be attributed to RE-oxide precipitates and their associated strain fields. Fitting Eq. (7) to the experimental data yielded characteristic temperatures $T_0 = 9$–13 K for the weak pinning centers and $T^* = 78$–81 K for the pinning energy scale of an isolated strong correlated defect.[50]

C. Magnetic relaxation of J_c with time

To probe further the pinning and dynamics of vortices in these materials, we measured the decay with time of the persistent current density at temperatures $T = 5$–77 K in magnetic fields of 1 and 3 T using SQUID magnetometry. Representative results for $J(t)$ at 40 and 70 K at 1 T are displayed in Fig. 7 in log-log format. As can be seen in Fig. 7(a), there is a logarithmic variation with time for all three samples at 40 K; here the relaxation rate $S = -d \ln J/d \ln t$ is almost the same for three samples, ~ 0.031. At 70 K, however,
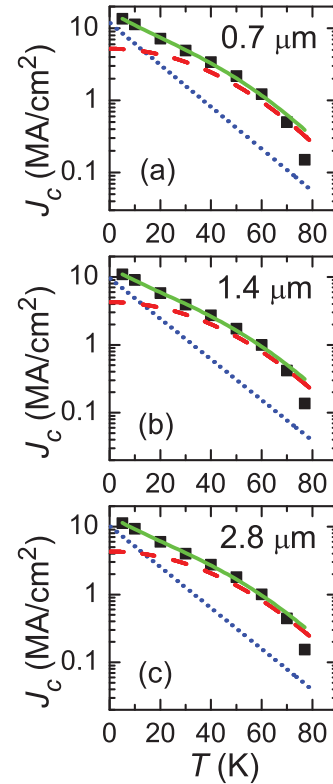

FIG. 6. (Color online) Partitioning of J_c measured at 1 T into weak pinning (dotted line) and strong pinning (dashed line) components by fitting its temperature dependence as described in the text. Solid line shows overall fit to the experimental data. For all investigated samples of (a) 0.7 μm, (b) 1.4 μm, and (c) 2.8 μm thickness, the strong pinning component is largest at most temperatures.

the differences in relaxation rates are more pronounced, as shown in Fig. 7(b). For the thinnest sample, 0.7 μm, the relaxation curve has become distinctly nonlinear as this material approaches its irreversibility line. For conditions much farther from the irreversibility line, Thompson *et al.* have demonstrated in long-term relaxation studies (orders of days) that the decay of $J(t)$ is nonlogarithmic in time.[56,57] This phenomenon is well described by the "interpolation formula,"[58]

$$J(T,t) = \frac{J_{c0}}{\left[1 + \frac{\mu k_B T}{U_0} \ln\left(\frac{t}{t_0}\right)\right]^{\frac{1}{\mu}}}.$$ (8)

We shall discuss this formula in detail below.

The logarithmic decay rate S, defined as [59]

$$S = -\frac{d \ln(J)}{d \ln(t)} = -\frac{d \ln(M_{\text{irr}})}{d \ln(t)} \approx -\frac{1}{M_{\text{irr}}} \frac{d M_{\text{irr}}}{d \ln(t)},$$ (9)

corresponds to the slope of the curves in Figs. 7(a) and 7(b). The temperature dependence of S for the samples of three thicknesses is shown in Figs. 8(a) and 8(b) for applied fields of 1 and 3 T, respectively. In each figure there are three distinctive regions, with similar behavior for all samples. At low temperatures of 5–20 K, S increases approximately linearly with T. At intermediate temperatures 20–50 K, S is nearly constant and has similar values for the
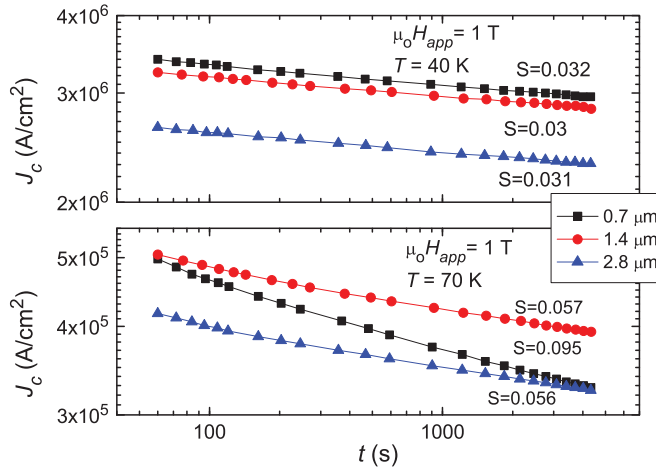
FIG. 7. (Color online) Decay of the current density with time (flux creep) for the materials with thicknesses indicated, in a 1 T magnetic field, $H \parallel$ surface-normal. Results are shown in log-log plots (a) at an intermediate temperature 40 K and (b) at high temperature 70 K. Values for the normalized creep rate $S = -d\ln(J)/d\ln(t)$ were obtained from slopes in plots like these.

three materials. For these reasons, the region is known as the "universal plateau."[59] The interpolation formula accounts for these features. By substituting Eq. (8) into Eq. (9) we obtain

$$S = \frac{k_B T}{U_0 + \mu k_B T \ln(t/t_0)}. \tag{10}$$

This equation predicts that the creep rate S increases linearly at low temperatures where the pinning energy scale $U_0 \gg T$ is dominant in the denominator; this leads to $S \approx (k_B T)/U_0$, which was also predicted in the earlier Anderson-Kim model. At higher temperatures the situation reverses when T term is larger than the pinning energy scale U_0, since the latter is also expected to decrease as T increases. Then one has

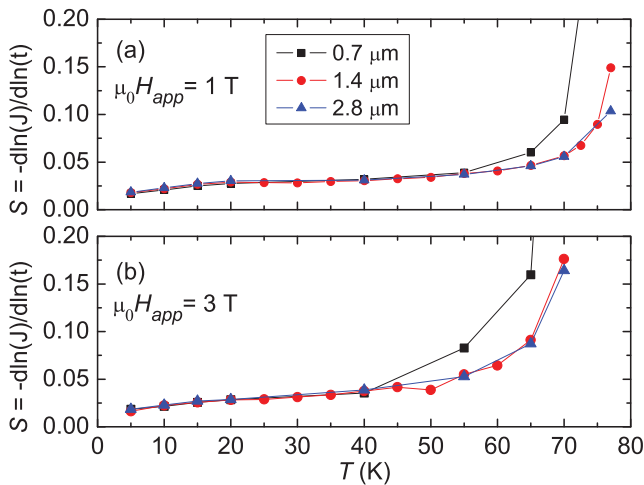$$S \approx \frac{1}{\mu \ln(t/t_0)}, \tag{11}$$

FIG. 8. (Color online) The creep rate S vs temperature T, measured in (a) 1 T applied field and (b) 3 T applied magnetic field, $H \parallel$ surface-normal.

which nicely accounts for the plateau region in the S vs T figures. In this region, the glassy exponent $\mu \approx$ constant and S becomes temperature independent.

At still higher temperatures, $T > 55$ K in Fig. 8, the relaxation rate S increases as thermal effects weaken the pinning, the current density decreases, and the underlying vortex dynamics evolve towards the eventual irreversibility line. In this higher temperature region the creep rate is notably faster for the thinnest sample. Values of S for the sample of intermediate thickness, 1.4 μm, *slightly* exceed those of the 2.8 μm material but are comparable. Overall, the magnetic relaxation rates are very similar at lower temperatures, but exhibit some dependence on thickness for higher temperature, higher field conditions.

As summarized recently by Maiorov *et al.*,[60] flux creep measurements are an ideal tool for exploring the depinning of vortices in various pinning landscapes, "particularly to identify the presence of columnar defects." Such defects manifest themselves as a pronounced peak[61] in S near 20–30 K, as Maiorov *et al.*[60] observed for BaZrO$_3$-doped YBCO films deposited at higher temperatures that promote the self-assembly of columns and as we reported for BaSnO$_3$ and other self-assembling dopants in coated conductors.[62] The absence of such a peak in Fig. 8 indicates once again that c axis correlated disorder contributes little to vortex pinning in the present materials. Instead, the overall behavior in Fig. 8 is comparable with that exhibited by point-defected (proton irradiated) single crystals[63] and YBCO films with no added phases for columnar defect formation;[60] very similar features include the presence of a plateau (rather than a peak) with comparable S values near 0.025–0.030, and accelerating creep rates at higher temperatures.

As input for the modeling of E-J curves to be discussed below, we have determined the scale of the pinning energy $U_0(T = 0)$. To do so we use the Anderson-Kim-like creep relation that provides $U_0(0) = {}^{\Delta T}/_{\Delta S}$ when T is small. From the slopes of the curves for $S(T)$ at low temperature, one obtains (for $H = 1$ T) the values $U_o(T = 0) = 1220$, 1150, and 1090 K for the 0.7, 1.4, and 2.8 μm thick films, respectively.

Now let us focus on the effective pinning energy $U_{\text{eff}}(J,T)$ that interacting vortices must overcome to hop from one pinning site to another. The original Anderson-Kim model assumed a simple linear dependence between U_{eff} and J, where J is less than but comparable with J_c. However, it has been shown both experimentally and theoretically that this model is inadequate for describing creep in HTS materials where thermal energies can be high, vortex interactions strong, and current densities $J \ll J_c$. Subsequently, vortex-glass theory[27–30] and collective creep theory[26] deduced similar power-law expressions for the effective pinning energy, with

$$U_{\text{eff}}(J,T) = U_0(T)\left[\left(\frac{J_c}{J}\right)^{\mu} - 1\right]. \tag{12}$$

Here μ is an important glassy exponent, whose theoretical value depends on the operative pinning process. The "Maley analysis" is the best known method for determining U_{eff} experimentally and it is described next.

D. Maley analysis

In order to obtain U_{eff} experimentally, Maley *et al.* developed a useful analysis.[64] This method is effectively based on a relaxation time approximation[49] where

$$dJ/dt = -\left(\frac{J_c}{\tau}\right)\exp\left[-\frac{U(J,T)}{T}\right] \qquad (13)$$

and τ is an unknown, but macroscopic attempt time for vortex hopping. In the Boltzmann factor we set $k_B = 1$ everywhere so that energies are measured in units of Kelvins. Solving Eq. (13) for U_{eff} gives

$$U_{\text{eff}} = -T\left(\ln\left|\frac{dJ}{dt}\right| - C\right),$$

where $C = \ln(J_c/\tau)$ is an unknown factor that is nominally constant at low temperatures where fundamental parameters such as the penetration depth and coherence length vary very little. Operationally, the factor C is the only unknown in this expression and its value is varied so as to produce a smooth, quasicontinuous curve of U_{eff} vs J at low temperatures, as shown in Fig. 9. Similar values, $C \approx 25$–27 as given in Fig. 9, were obtained for the three thicknesses. Figures 9(a)–9(c) show results for $U_{\text{eff}}(J,T)$ vs J, plotted as open symbols using logarithmic axes.

For further insight, it is useful to isolate the pinning energy's dependence on J from the effects of the temperature. To do so we assume that these variables are separable, at least approximately, and write

$$U_{\text{eff}}(J; T = 0) \approx U_{\text{eff}}(J; T)\big/G(T)$$

$$= -T\left(\ln\left|\frac{dJ}{dt}\right| - C\right)\Big/G(T).$$

The thermal function $G(T)$ accounts for various temperature dependencies, for example, for fundamental parameters like the coherence length and penetration depth, and it serves to establish a piecewise continuity of $U_{\text{eff}}(J)$ under conditions of lower J and elevated temperatures. The functional form $G(T) = (1 - T/T_c)^2$ was chosen empirically. The results for $U_{\text{eff}}(J; T = 0)$ are shown as filled symbols in Fig. 9. It can be seen that U increases as J decreases, in qualitative agreement with Eq. (12). When $J \ll J_c$, this equation gives a simple power-law dependence, as illustrated by the straight lines in Figs. 9(a)–9(c); this behavior persists for temperatures in the range 15–50 K. [At lower temperatures J approaches $J_c(T = 0)$ and Eq. (12) develops curvature.] The straight lines in Fig. 9 correspond to values for the glassy exponent μ of 1.7, 1.75, and 1.65 for films of 0.7, 1.4, and 2.8 μm thickness, respectively, all in 1 T fields applied parallel to the c axis. [Note that the value for μ at each temperature is defined by the slope of an individual segment in Fig. 9 and does *not* depend on the choice of the thermal function $G(T)$.] These values for μ lie near the theoretical value of 3/2 for hopping of small vortex bundles pinned collectively. Vortex-glass and collective creep theories predict many different glassy exponents for various regimes of vortex pinning and hopping. For example, vortex-glass theory has that μ is $\leqslant 1$. For collective pinning by weak point-like disorder, one has $\mu = 1/7$ for pinning of individual flux lines; in higher fields and temperatures where J is
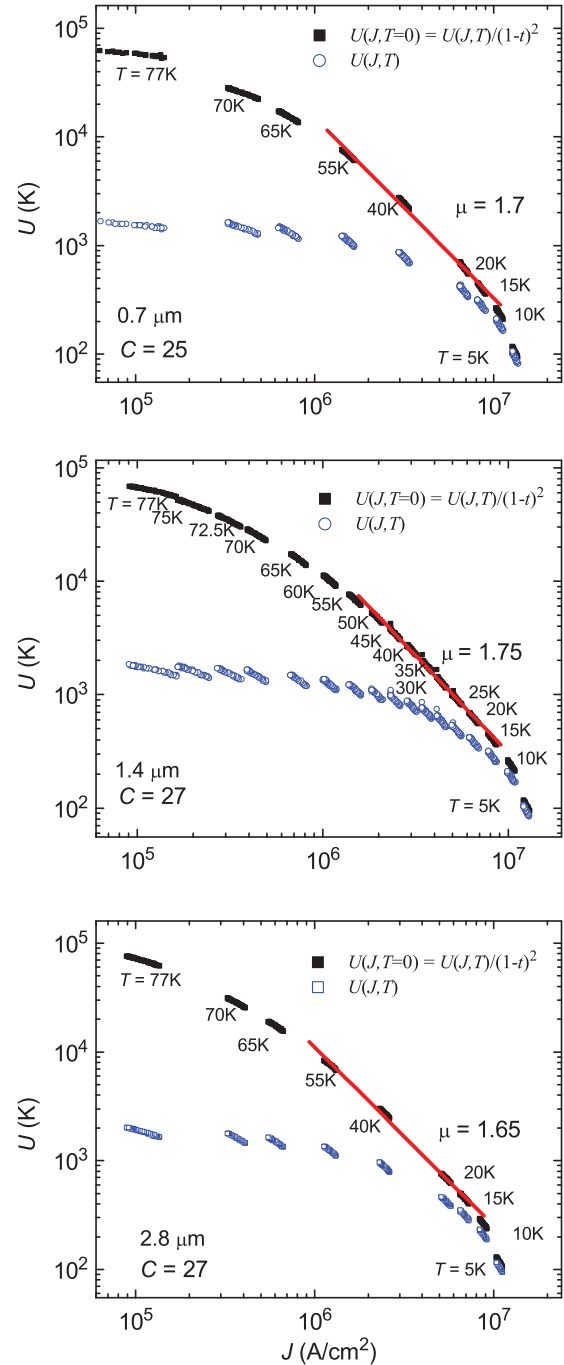

FIG. 9. (Color online) Current dependence of the effective pinning energy, as determined using a Maley analysis. A magnetic field of 1 T was applied to (a) 0.7 μm, (b) 1.4 μm, and (c) 2.8 μm thick films. Open symbols show $U_{\text{eff}}(J; T)$, where J was measured in magnetization measurements at the temperatures indicated in the figures. Filled symbols show the effective pinning energy with temperature effects factored out as $U_{\text{eff}}(J; T = 0) \approx U_{\text{eff}}(J; T)\big/G(T)$; see text. Solid straight lines show that a single glassy exponent $\mu \approx 1.7$ characterizes the three systems in the range ~15–50 K.

smaller and small bundles of flux are pinned, one has $\mu = 3/2$; for still smaller J with pinning of large bundles of flux at higher fields and temperatures, μ decreases to 7/9. Experimentally, a similar mechanism appears to be dominant up to ~50 K for all thicknesses 0.7–2.8 μm; at

higher temperatures the μ values decrease and vortex motion becomes progressively easier until the irreversibility line is reached.

Having deduced the glassy parameter μ applicable in the creep rate plateau region, one can also estimate the macroscopic time scale[49] t_0 for vortex hopping using the creep rates in Fig. 8(a). In particular, Eq. (11) provides that in the plateau region where $\mu T > U_0$, one has $\ln(t/t_0) = 1/(\mu S)$. To logarithmic accuracy this gives the value $t_0 \sim 10^{-6}$ s for all samples in 1 T applied magnetic field. This result, which is very comparable in magnitude with the theoretical estimate in Blatter *et al.*,[49] for these experimental conditions, will be used for modeling of the E-J curves in Sec. III F. For comparison, the macroscopic attempt time τ in Eq. (13) can be estimated using the experimental result $C = \ln(J_c/\tau) \approx 27$, giving $\tau \sim 8 \times 10^{-6}$ s. This value is similar to that found for t_0. Theoretically, these time scales are related[49] as $(t_0/\tau) = T|\partial J/\partial U|/J_{c0} = (J_c/J_{c0})(T/\mu U)$. Inserting experimental values, for example, at $T = 40$ K, from the Maley analysis and the following section gives $(t_0/\tau) \sim 2 \times 10^{-2}$ rather than ~ 1. This difference shows that establishing the appropriate time scales in vortex dynamics remains somewhat tenuous. Fortunately, the values are needed only to logarithmic accuracy.

E. *E-J* characteristics

Studies of the dependence of electric field on current density—the *E-J* characteristics—are useful for investigating vortex dynamics in superconductor materials. In this work *E-J* data spanning ~ 8 decades of dissipation are obtained from a combination of transport, swept field magnetometer, and flux creep measurements. In order to avoid sample-to-sample variations, the same samples were used for both VSM and SQUID measurements. The transport data were collected from samples cut from the same tapes, but they were of necessity physically and geometrically different from those investigated by magnetometry.

Figure 10 shows illustrative *E-J* characteristics at 77 K for the thickest sample, 2.8 μm, in log-log axes. Note the wide range of electric fields spanned by the several experimental methods. The transport measurements have the highest E fields near ~ 1 μV/cm. The magnetometers have different inherent electric field levels, for example, due to the accessible sweep rate for the magnetic field in the VSM. For the swept field measurements, J and E values were calculated by Eqs. (1) and (2), respectively; here the induced E field on the perimeter of the films was about 10^{-7}–10^{-9} V/cm. The $E(J)$ curves from the flux creep data were extracted using Eq. (3). The creep studies give the lowest electric fields, $E \sim 10^{-10}$–10^{-13} V/cm. For the two contact-free magnetic studies, the results correspond very well, while the transport data are offset by $\sim 25\%$ for the specific samples studied. Examination of Fig. 10 reveals that for individual segments there is a linear relation between E and J when plotted on log-log scales. This linearity shows that the *E-J* relation can be approximated by a power-law relation $E \propto J^n$ where n is the power-law index.

Contact-free magnetic measurements allow facile investigations of superconductive properties at low temperatures and high magnetic fields, which is a significant advantage over normal transport methods. Figure 11(a) shows results for
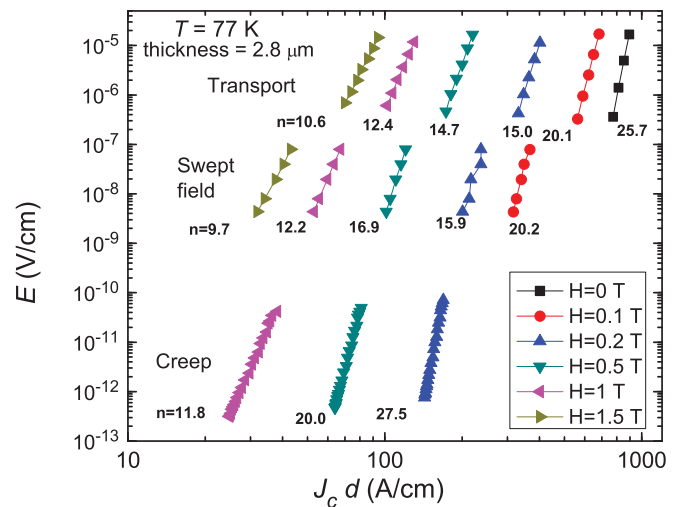

FIG. 10. (Color online) Electric field E vs current per unit width $J \times d$, where d is thickness of the film, for 2.8 μm thick film at 77 K, as obtained from a combination of transport, swept field VSM, and SQUID magnetometry. Values for the power-law index n, where $E \propto J^n$, were determined from slopes in the log-log plots.

temperatures from 5 to 77 K, for the 2.8 μm thick film in a fixed 1 T magnetic field applied parallel to the c axis. In Fig. 11(b) are shown *E-J* characteristics for samples of the three thicknesses, all at 77 K in a 1 T applied field. Here the thinnest film 0.7 μm has lower n values in the same operating conditions, compared to the other samples. It can be seen that as the temperature decreases, the current density becomes large and the n value increases. Clearly there are significant deviations from a simple power-law dependence at 77 K for conditions approaching the irreversibility line. Other deviations can be observed in Fig. 10 at 77 K, too. These deviations may be explained by J-dependent crossover in vortex pinning mechanism.

From Figs. 10 and 11 one can see that the *E-J* curve changes from convex at high J to concave curvature in the
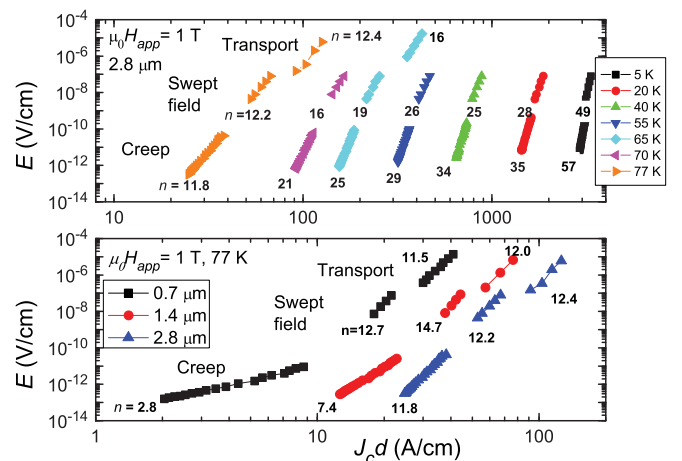

FIG. 11. (Color online) (a) Electric field-current characteristics, E vs $J \times d$, were determined at low temperatures by VSM and SQUID magnetometry measurements in the presence of a magnetic field $H = 1$ T applied along the c axis for 2.8 μm thick film. (b) Compares results for materials with various thicknesses at 77 K. Corresponding n values are shown.
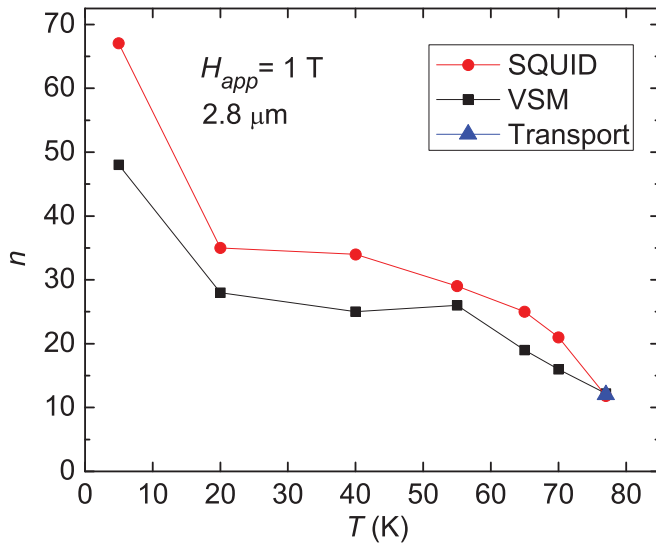
FIG. 12. (Color online) Values for the power-law index n extracted from transport, swept field VSM, and SQUID-based magnetometry vs operating temperature T, in 1 T applied magnetic field. The power index n is inversely proportional to the creep rate S, $n \sim 1/S$, as can be seen qualitatively by comparing this figure with Fig. 8.
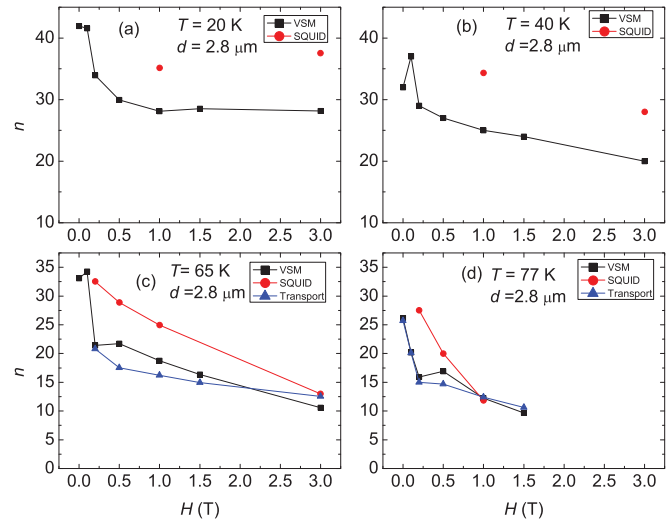

FIG. 13. (Color online) The magnetic field dependence of the n values for 2.8 μm thick film were determined from swept field VSM, and SQUID-based magnetometry at (a) 20 K and (b) 40 K. Values for n (c) at 65 K and (d) at 77 K were obtained from transport, swept field VSM, and SQUID-based magnetometry. The n values decrease with increasing temperature and applied magnetic field.

lower J region, with a crossover that depends on the applied field and operating temperature. The downward curvature is predicted by the vortex-glass theory[27–30] and collective flux creep theory,[25,26] in which the effective pinning energy has the form of $U(J) \cong U_0(J_0/J)^\mu$. In the limit of $J \to 0$, the pinning energy $U(J) \to \infty$, meaning that the E-J curves become gradually steeper. In other words, this behavior is "glassy." In this case where $U(J) \to \infty$, vortex hopping to neighboring sites becomes impossible.

Now we consider the power-law index n because it reflects the vortex state properties of a material, and it is as well as important engineering parameter for superconductor applications. The n value can be determined from the slope of the E-J curves, $n = d\ln(E)/d\ln(J)$ at different magnetic fields and temperatures. The temperature dependence of n values for the 2.8 μm thick material at 1 T is presented in Fig. 12. Data were extracted from creep, swept field, and transport studies. For creep studies, Yamasaki *et al.*[65] have shown an inverse relation between the creep rate S and power-law index n, with $S = 1/(n\text{-}1)$, Qualitatively, this relation can be visualized comparing Figs. 8 and 12. In Fig. 12 the n values increase with decreasing temperature, underscoring the progressive steepening of E-J curves seen in Figs. 10 and 11. The field dependence of n is shown in Figs. 13(a)–13(d) for representative temperatures. The n values generally decrease with temperature and applied magnetic field, becoming small at high temperature and high magnetic fields. Figure 14 shows the thickness dependence of n values for the three samples at different temperatures in 1 T magnetic field, for VSM and SQUID measurements, respectively. At the lowest temperature, all samples exhibit large n values, while a plateau region is observed at intermediate temperatures (20–55 K) for both VSM and SQUID measurements. This plateau is, of course, the same "universal plateau" observed in the plot of S vs T in Fig. 8. Finally, the thicker films have higher n values at

high temperatures, $T > 55$ K, that is, the conditions envisioned for technological application of such materials.

To gain perspective on the various results for n values in Figs. 12–14, it is important to recall that n is the slope of the (logarithmic) $E(J)$ curves, which reflect the underlying vortex pinning properties of the material. Thus n tends to trend to lower values with increasing temperature or magnetic field. Qualitatively, pinning will be weakened, creep accelerated, and n diminished if the vortex longitudinal correlation length (which generally increases with temperature) exceeds the film thickness, suggesting a more rapid deterioration of properties for the thinnest material, as observed. Finally, glassiness in the vortex system means that the bundle size and pinning energy grow as J decreases, causing the $E(J)$ curves to be
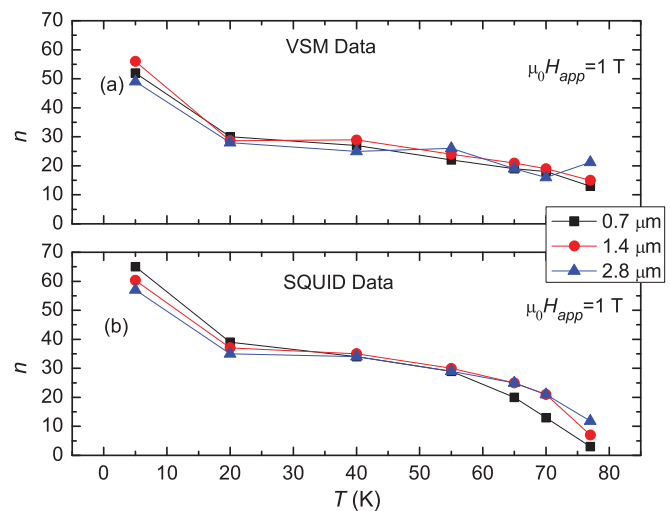

FIG. 14. (Color online) Temperature dependence of n values for the three thickness materials, as obtained using (a) VSM and (b) SQUID magnetometry.
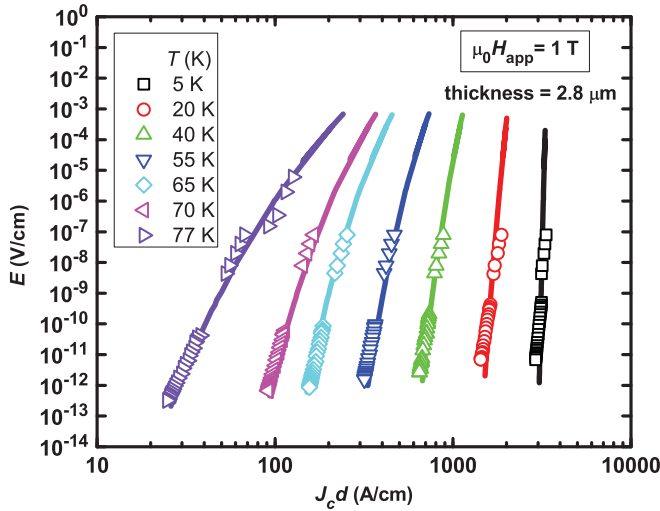
FIG. 15. (Color online) Modeling of electric field E vs current per width $J \times d$ in a 1 T field, for $T = 5$–77 K. Discrete symbols show experimental results over a wide range of dissipation; solid lines show modeling as described in the text.

concave downward. Thus the largest values for n are found for the experimental method (SQUID) with the lowest electric field level, and vice versa. The glassy, downward curving $E(J)$ characteristics are particularly visible and explored in the next section.

F. Modeling of E-J characteristics

In this section, we model the experimentally observed $E(J)$ data for a broad temperature range up to the glass temperature. The model is based on the formulation of vortex dynamics that has been developed since the advent of HTS materials. To begin, recall that thermally activated depinning causes the current density to decay with time. It has been shown theoretically and experimentally that the time dependence $J(t)$ is well described by the "interpolation formula," Eq. (8). The resulting electric field E on the perimeter of the sample is given by Eq. (3) for the creep measurements. Substituting Eq. (8) into Eq. (3) gives the following:

$$E\left(t\right) = \frac{\pi}{12}\mu_0 a d \frac{J_{c0}T}{U_0 T\left[1 + \left(\frac{\mu T}{U_0}\right)\ln\left(\frac{t}{t_0}\right)\right]^{(1+1/\mu)}}. \quad (14)$$

With Eqs. (8) and (14) one can obtain E vs J numerically by varying the time t as a "dummy" variable, producing curves like the solid lines shown in Fig. 15. Of the four parameters in total, three have already been determined for these materials. First, we have found for the macroscopic time scale that $t_0 \sim 10^{-6}$ s. In addition, the scale of pinning energy at $T = 0$, $U_0(0)$, was extracted from the creep analysis at low temperatures; at higher temperatures, we estimate the pinning energy as $U_0(T) = U_0(0)[1 - (T/T_c)^2]$. Finally, values for the glassy exponent μ at each temperature [Fig. 16(a)] were obtained from the Maley analysis shown in Fig. 9. Consequently, the only unknown parameter is the current density in the absence of flux creep J_{c0} and this prefactor was varied manually to best describe the experimentally observed $E(J)$ characteristics.
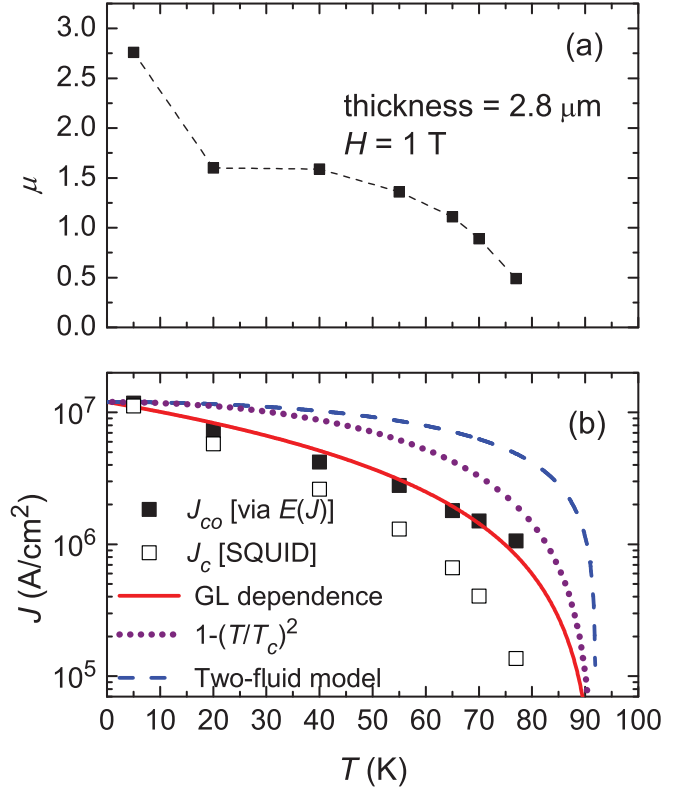

FIG. 16. (Color online) (a) Values for the glassy exponent μ, obtained from a Maley analysis and used to model the E-J curves in Fig. 15. (b) Temperature dependence of the critical current density J_{c0} (filled squares) at 1 T in the absence of flux creep, obtained via modeling of the E-J curves. For comparison, open squares show experimental values measured initially by SQUID magnetometry. Solid, dotted, and dashed lines show simple Ginzburg-Landau, BCS-like, and two-fluid temperature variations, respectively.

The results of this modeling are shown in Fig. 15 for the 2.8 μm thick film in a 1 T applied magnetic field, for temperatures of 5–77 K. It is seen that the modeling describes the experimentally determined $E(J)$ characteristics reasonably well at temperatures above $\sim$20 K.

Now, let us examine the temperature dependence of $J_{c0}(T)$, the critical current density in the absence of flux creep, as obtained from the $E(J)$ modeling and plotted in Fig. 16(b) for the 2.8 μm thick sample. At first sight, the falloff with temperature is surprising, particularly at lower temperatures. To explore and analyze this dependence in the absence of a known, specific theoretical expression applicable to the materials studied, we assume that J_{c0} varies with temperature in a manner similar to the depairing current density. From GL theory, one has

$$J_{\text{dep}}\left(T\right) \approx \frac{H_c}{\lambda} \cong \frac{1}{\lambda^2 \xi},$$

where $\lambda(T)$ and $\xi(T)$ are the penetration depth and coherence length, respectively. A simple possibility for their temperature dependence is a GL form with $\lambda^{-2}(T) \sim (1-T/T_c)$ and $\xi^{-2}(T) \sim (1-T/T_c)$. While this linear variation is normally considered to be valid only for some region around T_c, it faithfully describes some materials over a remarkably wide

temperature range of applicability.[66] With this dependence, one has $J_{c0}(T) \propto J_{\text{dep}}(T) \approx (1 - T/T_c)^{3/2}$. The solid red curve in Fig. 16(b) shows this form fitted to the deduced values for $J_{c0}(T)$, whose variation with temperature is described surprisingly well. Other temperature dependencies for the penetration depth provide contrasting cases, for example, $\lambda^{-2}(T) \sim [1-(T/T_c)^m]$, where $m = 2$ or 4 for BCS-like or two fluid models, respectively. These make $J_{c0}(\text{T})$ flat at low temperatures, as shown by the dotted and dashed lines in Fig. 16(b) that do not describe the $J_{c0}(T)$ results. Other more elaborate theoretical or empirical expressions for the current density might be considered, of course. Here, however, we wish mainly to illustrate that the surprising falloff in $J_{c0}(T)$, a quantity that is difficult to access experimentally, can be visualized qualitatively using well recognized dependencies.

IV. CONCLUSIONS

We have investigated the dependence of J_c in (Gd-Y)-Ba-Cu-O thin films, grown on IBAD templates, as a function of thickness, field magnitude, and temperature. Generally the J_c decreases somewhat with thickness for all applied fields and operating temperatures. Otherwise, the most notable variation with decreasing thickness is an apparent reduction in the irreversibility field, which affects the observed values for the power-law index α at high temperatures. For the most part, however, values for α, which describes the falloff of current density at intermediate fields, lie in the theoretically predicted range $\sim 5/8$ to $1/2$ for pinning by noncorrelated, nominally isotropically shaped defects. An analysis of the temperature

dependence of J_c points to a predominance of strong vortex pinning at all thicknesses for these materials. Other analyses of pinning showed little variation with thickness, for example, in the Maley analysis where similar values for the glassy exponent $\mu \approx 1.7$ were found. Expressed differently, the vortex pinning properties of these sequentially deposited materials appear to be rather uniform and exhibit no notable evolution with thickness in the range studied.

By combining conventional transport methods, field swept magnetometry, and flux creep studies, the voltage-current $E(J)$ characteristics were determined for a wide range of dissipation levels. A self-consistent modeling of the $E(J)$ characteristics was developed, based on standard results from "glassy" vortex dynamics. The only unconstrained parameter was the critical current density in the absence of flux creep $J_{c0}(T)$. Overall, this work shows that concepts of glassy vortex dynamics, which were developed for fundamental understanding of high-T_c superconductors, can provide important insights in coated conductors for technological applications.

*jrt@utk.edu

[1] F. E. Luborsky, R. F. Kwasnick, K. Borst, M. F. Garbauskas, E. L. Hall, and M. J. Curran, J. Appl. Phys. **64**, 6388 (1988).

[2] S. R. Foltyn, P. Tiwari, R. C. Dye, M. Q. Le, and X. D. Wu, Appl. Phys. Lett. **63**, 1848 (1993).

[3] C. Jooss, A. Forkl, and H. Kronmuller, Physica C **268**, 87 (1996).

[4] F. Laviano, D. Botta, R. Gerbaldo, G. Ghigo, L. Gozzelino, L. Gianni, S. Zannella, and E. Mezzetti, Physica C **404**, 220 (2004).

[5] S. R. Foltyn, L. Civale, J. L. MacManus-Driscoll, Q. X. Jia, B. Maiorov, H. Wang, and M. Maley, Nat. Mater. **6**, 631 (2007).

[6] M. Paranthaman, C. Park, X. Cui, A. Goyal, D. F. Lee, P. M. Martin, D. T. Verebelyi, D. P. Norton, D. K. Christen, and D. M. Kroeger, J. Mater. Res. **15**, 2647 (2000).

[7] S. R. Foltyn, Q. X. Jia, P. N. Arendt, L. Kinder, Y. Fan, and J. F. Smith, Appl. Phys. Lett. **75**, 3692 (1999).

[8] D. M. Feldmann, D. C. Larbalestier, R. Feenstra, A. A. Gapud, J. D. Budai, T. G. Holesinger, and P. N. Arendt, Appl. Phys. Lett. **83**, 3951 (2003).

[9] A. O. Ijaduola, J. R. Thompson, R. Feenstra, D. K. Christen, A. A. Gapud, and X. Song, Phys. Rev. B **73**, 134502 (2006).

[10] B. W. Kang, A. Goyal, D. R. Lee, J. E. Mathis, E. D. Specht, P. M. Martin, D. M. Kroeger, M. Paranthaman, and S. Sathyamurthy, J. Mater. Res. **17**, 1750 (2002).

[11] D. M. Feldmann, D. C. Larbalestier, R. Feenstra, A. A. Gapud, J. D. Budai, T. G. Holesinger, and P. N. Arendt, Appl. Phys. Lett. **83**, 3951 (2003).

[12] R. Feenstra, A. A. Gapud, F. A. List, E. D. Specht, G. K. Christen, T. G. Holesinger, and D. M. Feldmann, IEEE Trans. Appl. Supercond. **15**, 2803 (2005).

[13] B. Maiorov, A. Kursumovic, L. Stan, H. Zhou, H. Wang, L. Civale, R. Feenstra, and J. L. MacManus-Driscoll, Supercond. Sci. Technol. **20**, S223 (2007).

[14] H. Wang, S. R. Foltyn, L. Civale, B. Maiorov, and Q. X. Jia, Physica C **469**, 2033 (2009).

[15] S. R. Foltyn, P. N. Arendt, Q. X. Jia, H. Wang, J. L. MacManus-Driscoll, S. Kreiskott, R. F. De Paula, L. Stan, J. R. Groves, and P. C. Dowden, Appl. Phys. Lett. **82**, 4519 (2003).

[16] S. R. Foltyn, H. Wang, L. Civale, B. Maiorov, and Q. X. Jia, Supercond. Sci. Technol. **22**, 125002 (2009).

[17] A. Gurevich, Supercond. Sci. Technol. **20**, S128 (2007).

[18] A. Sanchez, C. Navau, N. Del-Valle, D.-X. Chen, and J. R. Clem, Appl. Phys. Lett. **96**, 072510 (2010).

[19] J. R. Thompson, O. Polat, D. K. Christen, D. Kumar, P. M. Martin, and J. W. Sinclair, Appl. Phys. Lett. **93**, 042506 (2008).

[20] O. Polat, J. R. Thompson, D. K. Christen, D. Kumar, P. M. Martin, J. W. Sinclair, F. A. List, V. Selvamanickam, and Y. M. Chen, in *High Temperature Superconductors,* edited by R. Bhattacharya and

M. P. Paranthaman (Wiley-VCH, Weinheim, Germany, 2010), pp. 49–65.

[21] P. England, T. Wenkatesan, T. L. Cheeks, H. G Craighead, C. T. Rogers, and S. W. Chan, IEEE Trans. Magn. **25**, 2237 (1989).

[22] M. Sugahara, M. Kojima, N. Yoshikawa, T. Akeyoshi, and N. Haneji, Phys. Lett. A **125**, 429 (1987).

[23] P. C. E. Stamp, L. Forro, and C. Ayache, Phys. Rev. B **38**, 2847 (1988).

[24] N. C. Yeh and C. C. Tsuei, Phys. Rev. B **39**, 9708 (1989).

[25] M. Wallin and S. M. Girvin, Phys. Rev. B **47**, 14642 (1993).

[26] M. V. Feigel'man, V. B. Geshkenbein, A. I. Larkin, and V. M. Vinokur, Phys. Rev. Lett. **63**, 2303 (1989).

[27] M. P. A. Fisher, Phys. Rev. Lett. **62**, 1415 (1989).

[28] D. S. Fisher, M. P. A. Fisher, and D. A. Huse, Phys. Rev. B **43**, 130 (1991).

[29] R. H. Koch, V. Foglietti, W. J. Gallagher, G. Koren, A. Gupta, and M. P. A. Fisher, Phys. Rev. Lett. **63**, 1511 (1989).

[30] R. H. Koch, V. Foglietti, and M. P. A. Fisher, Phys. Rev. Lett. **64**, 2586 (1990).

[31] C. P. Bean, Rev. Mod. Phys. **36**, 31 (1964).

[32] A. M. Campbell and J. E. Evetts, Adv. Phys. **21**, 199 (1972).

[33] L. Krusin-Elbaum, L. Civale, J. R. Thompson, and C. Feild, Phys. Rev. B **53**, 11744 (1996).

[34] A. A. Babaei Brojeny and J. R. Clem, Supercond. Sci. Technol. **18**, 888 (2005).

[35] T. Aytug, M. Paranthaman, A. A. Gapud, S. Kang, H. M. Christen, K. J. Leonard, P. M. Martin, J. R. Thompson, D. K. Christen, R. Meng, I. Rusakova, C. W. Chu, and T. H. Johansen, J. Appl. Phys. **98**, 114309 (2005).

[36] T. Aytug, M. Paranthaman, K. J. Leonard, S. Kang, P. M. Martin, L. Heatherly, A. Goyal, A. O. Ijaduola, J. R. Thompson, D. K. Christen, R. Meng, I. Rusakova, and C. W. Chu, Phys. Rev. B **74**, 184505 (2006).

[37] F. Hengstberger, M. Eisterer, and H. W. Weber, Appl. Phys. Lett. **96**, 022508 (2010).

[38] A. Sanchez, C. Navau, N. Del-Valle, D. X. Chen, and J. R. Clem, Appl. Phys. Lett. **96**, 072510 (2010).

[39] D. V. Shantsev, Y. M. Galperin, and T. H. Johansen, Phys. Rev. B **61**, 9699 (2000).

[40] B. Dam, J. M. Huijbregtse, F. C. Klaassen, R. C. F. van der Geest, G. Doornbos, J. H. Rector, A. M. Testa, S. Freisem, J. C. Martinez, B. Stäuble-Pümpin, and R. Griessen, Nature (London) **399**, 439 (1999).

[41] Y. N. Ovchinnikov and B. I. Ivlev, Phys. Rev. B **43**, 8024 (1991).

[42] C. J. van der Beek, M. Konczykowski, A. Abal'oshev, I. Abal'osheva, P. Gierlowski, S. J. Lewandowski, M. V. Indenbom, and S. Barbanera, Phys. Rev. B **66**, 024523 (2002).

[43] Y. Zhang, E. Specht, C. Cantoni, D. K. Christen, J. R. Thompson, J. W. Sinclair, A. Goyal, Y. L. Zuev, T. Aytug, P. M. Paranthaman, Y. M. Chen, and V. Selvamanickam, Physica C **469**, 2044 (2009).

[44] B. Maiorov, B. J. Gibbons, S. Kreiskott, V. Matias, T. G. Holesinger, and L. Civale, Appl. Phys. Lett. **86**, 132504 (2005).

[45] L. Civale, B. Maiorov, J. L. MacManus-Driscoll, H. Wang, T. G. Holesinger, S. R. Foltyn, A. Serquis, and R. N. Arendt, IEEE Trans. Appl. Supercond. **15**, 2808 (2005).

[46] S. I. Kim, A. Gurevich, X. Song, X. Li, W. Zhang, T. Kodenkandath, M. W. Rupich, T. G. Holesinger, and D. C. Larbalestier, Supercond. Sci. Technol. **19**, 968 (2006).

[47] S. Senoussi, M. Oussena, G. Collin, and I. A. Campbell, Phys. Rev. B **37**, 9792 (1988).

[48] D. K. Christen and J. R. Thompson, Nature (London) **98**, 364 (1993).

[49] G. Blatter, M. V. Feigelman, V. B. Geshkenbein, A. I. Larkin, and V. M.Vinokur, Rev. Mod. Phys. **66**, 1125 (1994).

[50] D. R. Nelson and V. M. Vinokur, Phys. Rev. B **48**, 13060 (1993).

[51] T. Hwa, P. LeDoussal, D. R. Nelson, and V. M. Vinokur, Phys. Rev. Lett. **71**, 3545 (1993).

[52] C. J. van der Beek, M. Konczykowski, V. M. Vinokur, T. W. Li, P. H. Kes, and G. W. Crabtree, Phys. Rev. Lett. **74**, 1214 (1995).

[53] V. V. Moshchalkov, V. V. Metlushko, G. Güntherodt, I. N. Goncharov, A. Yu. Didyk, and Y. Bruynseraede, Phys. Rev. B **50**, 639 (1994).

[54] B. Martinez, X. Obradors, A. Gou, V. Gomis, S. Pinol, J. Fontcuberta, and H. Van Tol, Phys. Rev. B **53**, 2797 (1996).

[55] J. Plain, T. Puig, F. Sandiumenge, X. Obradors, and J. Rabier, Phys. Rev. B **65**, 104526 (2002).

[56] J. R. Thompson, Y. R. Sun, D. K. Christen, L. Civale, A. D. Marwick, and F. Holtzberg, Phys. Rev. B **49**, 13287 (1994).

[57] J. R. Thompson, Y. R. Sun, and F. Holtzberg, Phys. Rev. B **44**, 458 (1991).

[58] Y. Yeshurun, A. P. Malozemoff, and A. Shaulov, Rev. Mod. Phys. **68**, 911 (1996).

[59] A. P. Malozemoff and M. P. A. Fisher, Phys. Rev. B **42**, 6784 (1990).

[60] B. Maiorov, S. A. Baily, H. Zhou, O. Ugurlu, J. A. Kennison, P. C. Dowden, T. G. Holesinger, S. R. Foltyn, and L. Civale, Nat. Mater. **8**, 398 (2009).

[61] J. R. Thompson, L. Krusin-Elbaum, L. Civale, G. Blatter, and C Field, Phys. Rev. Lett. **78**, 3181 (1997).

[62] D. K. Christen and J. R. Thompson, reported at DOE Advanced Cables and Conductors Program Peer Review, Alexandria VA, 1 July 2010 and available at [http:www.htspeerreview.com. pdfs_presentations_day%203_strategic-research_8_SR_HTS_ Coated_Conductor_Characterization_and_Analysis.pdf].

[63] L. Civale, A. D. Marwick, M. W. McElfresh, T. K. Worthington, A. P. Malozemoff, F. H. Holtzberg, J. R. Thompson, and M. A. Kirk, Phys. Rev. Lett. **65**, 1164 (1990).

[64] M. P. Maley, J. O. Willis, H. Lessure, and M. E. McHenry, Phys. Rev. B **42**, 2639 (1990).

[65] Y. Yamasaki and Y. Mawatari, IEEE Trans. Appl. Supercond. **9**, 2651 (1999).

[66] J. R. Thompson, H. R. Khan, and K. J. Song, Physica C **272**, 171 (1996).